Correlated motions of successive amide N-H bonds in proteins

Philippe Pelupessy[a], Sapna Ravindranathan[b] & Geoffrey Bodenhausen[a,b,*]
[a]*Département de chimie, associé au CNRS, Ecole Normale Supérieure, 24 rue Lhomond, 75231 Paris cedex 05, France*
[b]*Institut de chimie moléculaire et biologique, Ecole Polytechnique Fédérale de Lausanne, BCH, 1015 Lausanne, Switzerland*

Abstract

New nuclear magnetic resonance (NMR) methods are described for the measurement of cross-correlation rates of zero- and double-quantum coherences involving two nitrogen nuclei belonging to successive amino acids in proteins and peptides. Rates due to the concerted fluctuations of two NH^N dipole-dipole interactions and to the correlated modulations of two nitrogen chemical shift anisotropies have been obtained in a sample of doubly labeled Ubiquitin. Ambiguities in the determination of dihedral angles can be lifted by comparison of different rates. By defining a heuristic order parameter, experimental rates can be compared with those expected for a rigid molecule. The cross-correlation order parameter that can be derived from a model-free approach can be separated into structural and dynamic contributions.

Abbreviations: NMR – nuclear magnetic resonance; DQ – double quantum; ZQ – zero quantum; SQ – single quantum; CSA – chemical shift anisotropy; DD – dipole-dipole; NOE – nuclear Overhauser enhancement.

Introduction

Relaxation phenomena in NMR can provide a great deal of insight into molecular dynamics (Daragan and Mayo, 1997). In proteins fast internal motions of the backbone are usually probed by determining the relaxation parameters of the amide nitrogen nuclei (Peng and Wagner, 1992). Typically, a set of transverse and longitudinal relaxation rates, complemented by the measurement of nuclear Overhauser enhancements (NOE) caused by saturation of the protons, are interpreted using the model-free approach (Lipari and Szabo, 1982). Transverse and longitudinal cross-correlation rates involving the N chemical shift anisotropy (CSA) and NH^N dipole/dipole (DD) interactions provide useful additional information (Tjandra et al., 1996; Kroenke et al., 1998). These parameters however are insufficient to fully determine local motion, since they are insensitive to rotations

about the NH^N vector and often cannot distinguish between different models. These problems can be alleviated by the measurement of C′ carbonyl relaxation parameters (Dayie and Wagner, 1995) and several cross-correlation rates such as C'/NH^N (CSA/DD) (Brutscher et al., 1998), $C'/C'H^N$ (CSA/DD) (Pang et al., 1999; Früh et al., 2002), C'/N (CSA/CSA) (Pang and Zuiderweg, 2000) and $NH^N/C'C^\alpha$ (DD/DD) (Carlomagno et al., 2000). These rates are sensitive to internal motions that are faster than or comparable to the global correlation time (Lipari and Szabo, 1982). Slower motions can be detected when the isotropic chemical shifts are modulated. The effect of such modulations on single quantum coherences can be observed by Carr–Purcell–Meiboom–Gill (CPMG) with variable repetition rates (Loria et al., 1999) or by spin-lock experiments (Akke and Palmer, 1996). Slow motions may also lead to differential relaxation between zero- and double quantum coherences (Wokaun

---

*To whom correspondence should be addressed.

and Ernst, 1978; Tessari and Vuister, 2000; Kloiber and Konrat, 2000b; Früh et al., 2001).

Cross-correlated relaxation rates can be used to determine Ψ-angles (Reif et al., 1997; Yang et al., 1997; Chiarparin et al., 1999) and Φ-angles (Pelupessy et al., 1999b; Kloiber and Konrat, 2000a) in proteins. Ambiguities inherent to these kinds of parameters can be overcome by measurements of additional rates such as those involving $C^\alpha H^\alpha/C^\alpha H^\alpha$ (DD/DD) interactions (Chiarparin et al., 2000) or C'/C' (CSA/CSA) (Skrynnikov et al., 2000) in successive residues. The effects of anisotropic tumbling (Deschamps and Bodenhausen, 2001), of local motions (Deschamps, 2002) and of conformational exchange (Tolman et al., 2000) on these rates have recently been investigated.

In this paper we introduce methodology to measure NH^N/NH^N (DD/DD) and N/N (CSA/CSA) cross-correlation rates of two-spin coherences involving two amide nitrogen nuclei in successive residues. These rates provide useful structural information, in addition to the previously mentioned rates. The methods are ideally suited for the study of local dynamics, since the results can be directly compared with those obtained for the well-studied single quantum relaxation rates of amide nitrogen nuclei (Tjandra et al., 1995).

Methodology

Figure 1 shows two pulse sequences which allow quantitative measurements of cross-correlation rates arising from correlated fluctuations of two NH^N DD interactions or of two nitrogen CSA's involving successive residues. The pulse sequence utilizes a cascade of four INEPT-like transfers in order to convert amide proton magnetization $H_y^N(i)$ into multiple spin coherence $8N_y(i)C_z^\alpha(i)C_z'(i)N_y(i+1)$, involving two nitrogen spins in successive residues. In the following, the position of the nuclei in the product operators reflects the order of the nuclei in the protein and we can therefore omit the indices (i) and $(i+1)$. After the relaxation period T the coherence is reconverted into observable amide proton magnetization by a sequence of reversed INEPT steps, mirror-imaging the first four steps.

Operators describing the relevant coherences at different stages in the sequence are indicated in the figure. The relaxation period T, as highlighted in frames, can be designed to measure either the DD/DD cross-correlation rates between two NH^N vectors or the CSA/CSA cross-correlation rates associated with two nitrogen nuclei of successive residues. Under the influence of the DD/DD-interaction the coherence $8N_y C_z^\alpha C_z' N_y$ is partially transformed into $32N_x H_z^N C_z^\alpha C_z' N_x H_z^N$. At $T/4$ and $3T/4$, two π-pulses are applied to the protons to suppress the influence of DD/CSA cross-correlation mechanisms involving protons and nitrogens (Chiarparin et al., 1999). The nitrogen π-pulse refocuses the chemical shift evolution and various scalar coupling interactions.

Two experiments must be performed, one to detect the decay of the initial coherence (I) and the second to detect the coherence resulting from DD/DD cross-correlation (II). In experiment II the proton π-pulses are shifted by $1/(8^1 J_{NH})$ with respect to experiment I, in order to convert $32N_x H_z^N C_z^\alpha C_z' N_x H_z^N$ back into $8N_y C_z^\alpha C_z' N_y$. This scheme permits us to focus on identical coherences at the end of the relaxation period T in both experiments.

In addition to the coherences discussed above, other terms are created that result from long-range scalar couplings. Specifically, the second INEPT sequence which is intended to transfer from the nitrogen to the neighboring C^α will also lead to a partial transfer to the C^α of the preceding residue. The operators resulting from this unwanted pathway are indicated in brackets in figure 1. The two pathways cannot be separated by phase-cycling. However, the $\pi/2$ pulses flanking the relaxation period T do not affect the second pathway. Hence, by omitting the pulse indicated by an asterisk and inverting the receiver phase, the contribution of the undesired pathway can be eliminated (Chiarparin et al., 2000).

The sequence has to be slightly modified to measure the CSA/CSA cross-correlation rate which converts the coherence $8N_y C_z^\alpha C_z' N_y$ into $8N_x C_z^\alpha C_z' N_x$. In this case, proton decoupling is applied throughout the relaxation period T. In order to detect the coherence that is created by cross-correlation, one merely has to shift the phase of the nitrogen pulse marked with an asterisk by $90°$. Such experiments will be referred to as I' and II'.

Figure 2 depicts the main cross-correlation rates (Yang and Kay, 1998) that affect an $2N_y N_y$ two-spin coherence in a spin system containing two nitrogen and two proton nuclei. The rates can be divided into two groups. Group A involves DD/DD or CSA/CSA cross-correlations, while group B contains the CSA/DD rates. The DD interactions are indicated by bold lines between the nuclei and the CSAs by bold circles around the nuclei. Group A is effective during the entire relaxation period T, whereas the

$2N_yH_z \xrightarrow{\hspace{1cm}} 2N_zC_y^\alpha$

$\left\{ 2C_y^\alpha N_z \right.$

$2N_zC_z^\alpha C_y' \xrightarrow{\hspace{0.5cm}} 8N_yC_z^\alpha C_z'N_y$
$\qquad\qquad \Gamma'$
$\xrightarrow{\hspace{0.5cm}} 8N_yC_z^\alpha C_z'N_y$
$\qquad\qquad II'$
$\xrightarrow{\hspace{0.5cm}} \Gamma$
$8N_xC_z^\alpha C_z'N_x$

$4N_zC_z^\alpha C_y'$

$4C_z^\alpha C_y' N_z$

$8N_yC_z^\alpha C_z'N_y \xrightarrow{\hspace{0.5cm}} I$
$32N_xH_zC_z^\alpha C_z'N_xH_z$
$\xrightarrow{\hspace{0.3cm}} II$
Γ
$2C_z^\alpha C_z'$

$4N_zC_z^\alpha C_y' \xrightarrow{\hspace{0.5cm}} 2N_zC_y^\alpha$

$4C_z^\alpha C_y'N_z \xrightarrow{\hspace{0.5cm}} 2C_y^\alpha N_z \left. \right\} \xrightarrow{\hspace{0.5cm}} 2N_yH_z$
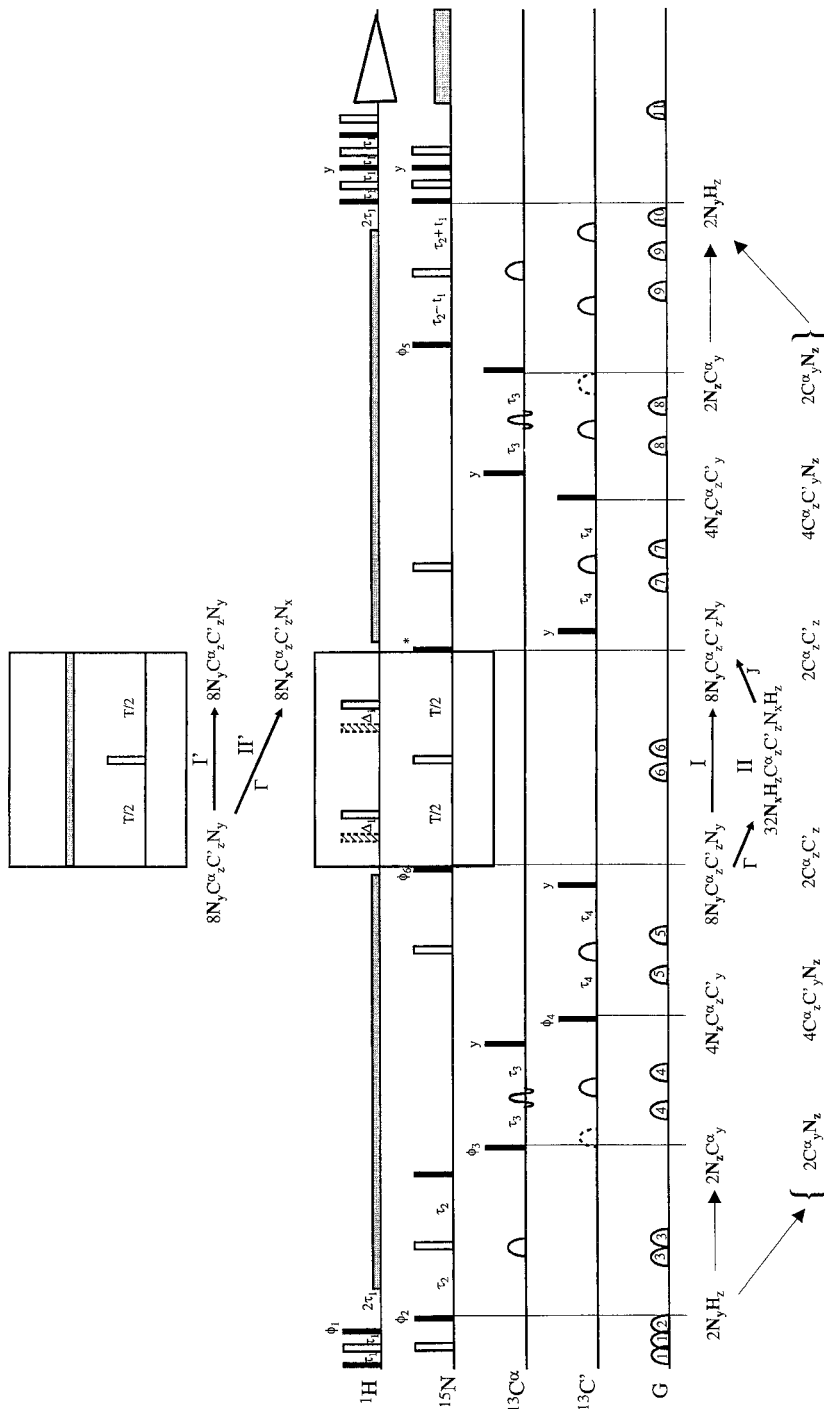
Figure 1. Pulse sequences employed to measure cross-correlation rates that affect two-spin coherences between amide nitrogen nuclei of successive amino-acids. Filled narrow and open wide rectangles indicate $\pi/2$ and π pulses. The C^α π refocusing pulses between the τ_3 intervals have RE-BURP profiles of 1.67 ms duration. All other π pulses on the C^α and C' have G3 profiles of 350 μs duration. The dashed pulses on the C' are for compensation of Bloch–Siegert phase-shifts. Very long gray rectangles indicate decoupling. The fixed delays are set to $\tau_1 = 1/(4 \, ^1J_{NH}) = 2.65$ ms, $\tau_2 = 15$ ms, $\tau_3 = 1/(4 \, ^1J_{C^\alpha C'}) = 4.55$ ms, $\tau_4 = (1/(4 \, ^1J_{NC'}) = 16.7$ ms. The ^{15}N evolution in the t_1 interval occurs in a constant time manner. Detection is achieved using echo/anti-echo gradient selection with sensitivity enhancement. On the lower bar the different gradients are indicated. Unless indicated otherwise, all pulses are applied along the x-axis. The phase cycle is: $\phi_1 = (y)$, $(-y)$, $\phi_2 = 2(x)$, $2(-x)$, $\phi_3 = 4(-x), 4(x)$, $\phi_4 = 8(x)$, $8(-x)$, $\phi_5 = 16(x)$, $16(-x)$, $\phi_6 = 32(x)$, $32(-x)$, $\phi_{rec} = (x, -x, -x, x)$, $2(-x, x, x, -x)$, $(x, -x, -x, x)$, $(-x, x, x, -x)$, $2(x, -x, -x, x)$, $(-x, x, x, -x)$. Below the sequence the relevant product operators are indicated. In the frames the relaxation period T is depicted. (Below) for the measurement of the NH^N/NH^N (DD/DD) and (top) for the N/N (CSA/CSA) cross-correlation rate. For both experiments a 'reference' (I) and a 'cross' (II) experiment are recorded. For the DD/DD experiment the proton π-pulses in the relaxation period T are shifted by $1/(8 \, ^1J_{NH})$ in experiment II in order to convert the product operator $32N_xH_zC_z^\alpha C_z'N_xH_z$ into $8N_yC_z^\alpha C_z'N_y$. For the CSA/CSA rate experiment I' is recorded with phase x for the pulse marked with an asterisk, while for experiment II' its phase is set to y. Between the accolades an undesired pathway is indicated which cannot be cancelled by a phase-cycle. In order to remove this pathway the pulse marked with an asterisk is dropped on alternating scans while inverting the receiver phase. As an alternative for the DD/DD experiment the phase of this pulse may be set to y on alternate scans, also inverting the receiver phase, in order to detect only the DQ coherences.

Table 1. Cross-correlated interactions which contribute to relaxation of two-spin coherences between two amide nitrogen nuclei in successive residues

R	Interaction	Operator[a]	Rate[b]
1	N(i)H(i),N(i+1)H(i+1)	$8N_x H_z N_x H_z$	$J(0)$
2	N(i)H(i+1),N(i+1)H(i)	$8N_x H_z N_x H_z$	$J(0)$
3	N(i),N(i+1)	$2N_x N_x$	$J(0)$
4	N(i)H(i),N(i+1)H(i)	$2N_x N_x$	$J(0) + \frac{3}{4}J(\omega_H)$
5	N(i)H(i+1),N(i+1)H(i+1)	$2N_x N_x$	$J(0) + \frac{3}{4}J(\omega_H)$
6	N(i)H(i),N(i)H(i+1)	$8N_y H_z N_y H_z$	$J(0) + \frac{3}{4}J(\omega_N)$
7	N(i+1)H(i),N(i+1)H(i+1)	$8N_y H_z N_y H_z$	$J(0) + \frac{3}{4}J(\omega_N)$
8	N(i),N(i)H(i)	$4N_y H_z N_y$	$J(0) + \frac{3}{4}J(\omega_N)$
9	N(i+1),N(i+1)H(i)	$4N_y H_z N_y$	$J(0) + \frac{3}{4}J(\omega_N)$
10	N(i),N(i)H(i+1)	$4N_y N_y H_z$	$J(0) + \frac{3}{4}J(\omega_N)$
11	N(i+1),N(i+1)H(i+1)	$4N_y N_y H_z$	$J(0) + \frac{3}{4}J(\omega_N)$
12	N(i),N(i+1)H(i)	$4N_x H_z N_x$	$J(0)$
13	N(i+1),N(i)H(i)	$4N_x H_z N_x$	$J(0)$
14	N(i),N(i+1)H(i+1)	$4N_x N_x H_z$	$J(0)$
15	N(i+1),N(i)H(i+1)	$4N_x N_x H_z$	$J(0)$

[a]Operator that is created by the interaction starting from an initial density operator $2N_y N_y$.

[b]Spectral density that contributes to the relaxation rate. The interaction constants are $\left(\frac{\mu_0 \hbar}{4\pi}\right)^2 \frac{\gamma_H^2 \gamma_N^2}{r_u^3 r_v^3}$, $\left(\frac{\mu_0 \hbar}{4\pi}\right) \frac{\gamma_H \gamma_N^2 2B_0 \Delta\sigma_u}{3r_v^3}$ and $\frac{\gamma_N^2 4B_0^2 \Delta\sigma_u \Delta\sigma_v}{9}$ for DD/DD, CSA/DD and CSA/CSA cross-correlation rates, respectively. The CSA is assumed to be axially symmetric. The spectral densities are defined in such a manner that $J(\omega) = P_2(\cos\Theta^{u,v})\frac{2}{5}\frac{\tau_c}{1+(\omega\tau_c)^2}$ for isotropic tumbling of a rigid molecule.

rates of group B are averaged out by the proton π-pulses, as can be seen in the 'toggling-frame' diagrams of Figure 2. The transformation of the initial density operator $2N_y N_y$ under the influence of the different interactions is given in Table 1. Mechanisms that lead to the same product operator are indistinguishable.

The ratio between the expectation values of the operator term created by cross-correlated relaxation and the initial density operator can be expressed by (Pelupessy et al., 1999a; Felli et al., 1999)

$$\frac{< 8N_x H_z^N N_x H_z^N >_{II}(T)}{< 2N_y N_y >_I (T)} = \tanh[(R_1 + R_2)T], \quad (1)$$

where R_1 and R_2 are given in Table 1. At longer relaxation times the product operator in the numerator might be also generated by two-step processes analogous to spin diffusion in NOESY. For example, $8N_x H_z^N N_x H_z^N$ can be also created by

$$2N_y N_y \xrightarrow{R_3+R_4+R_5} 2N_x N_x \xrightarrow{R_6+R_7} 8N_x H_z^N N_x H_z^N. \quad (2)$$

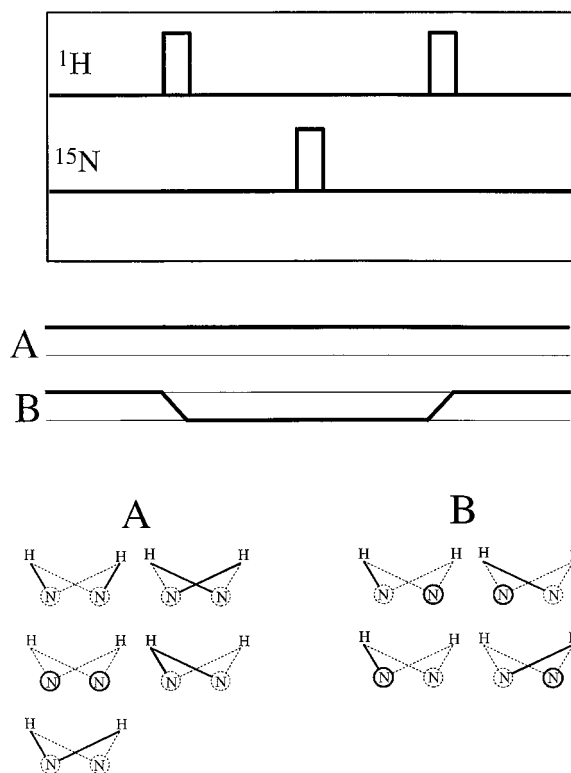Hence, Equation 1 is valid only when (Chiarparin, 2000):

Figure 2. Effect of different cross-correlation rates during the relaxation period T of Figure 1. The rates can be split into two groups: group A, that consists of DD/DD and CSA/CSA rates, is not affected by the π-pulses. The CSA/DD rates of group B are inverted by the proton π-pulses and their effect is nulled, as can be seen from the toggling-frame diagrams. All rates of Table 1 that can be represented by mirror-images of the pictograms with respect to a vertical plane have been omitted.

$$|R_3 + R_4 + R_5| \times |R_6 + R_7| \times T^2 \ll 1. \quad (3)$$

Another factor that should be considered is the *cross relaxation* rate σ_{HH} between the two amide protons. When the secular approximation holds (i.e., when $|^1J_{NH}(i) - {}^1J_{NH}(i + 1)| \gg |\sigma_{HH}|$), this rate causes a similar effect as R_6 and R_7 (Reiff et al., 2000). However, one-bond scalar couplings between amide protons and nitrogen nuclei are often similar. When $^1J_{NH}(i) \approx {}^1J_{NH}(i + 1)$, the cross relaxation rate σ_{HH} affects only the ZQ coherences and Equation (1) must be modified (see Appendix A):

$$\frac{< 8N_x H_z^N N_x H_z^N >_{II}(T)}{< 2N_y N_y >_I (T)} = \tanh\left[(R_1 + R_2 + \frac{1}{4}\sigma_{HH})T\right]. \quad (4)$$

Since DQ coherences are not affected by σ_{HH}, one can also redesign the experiment to detect only these
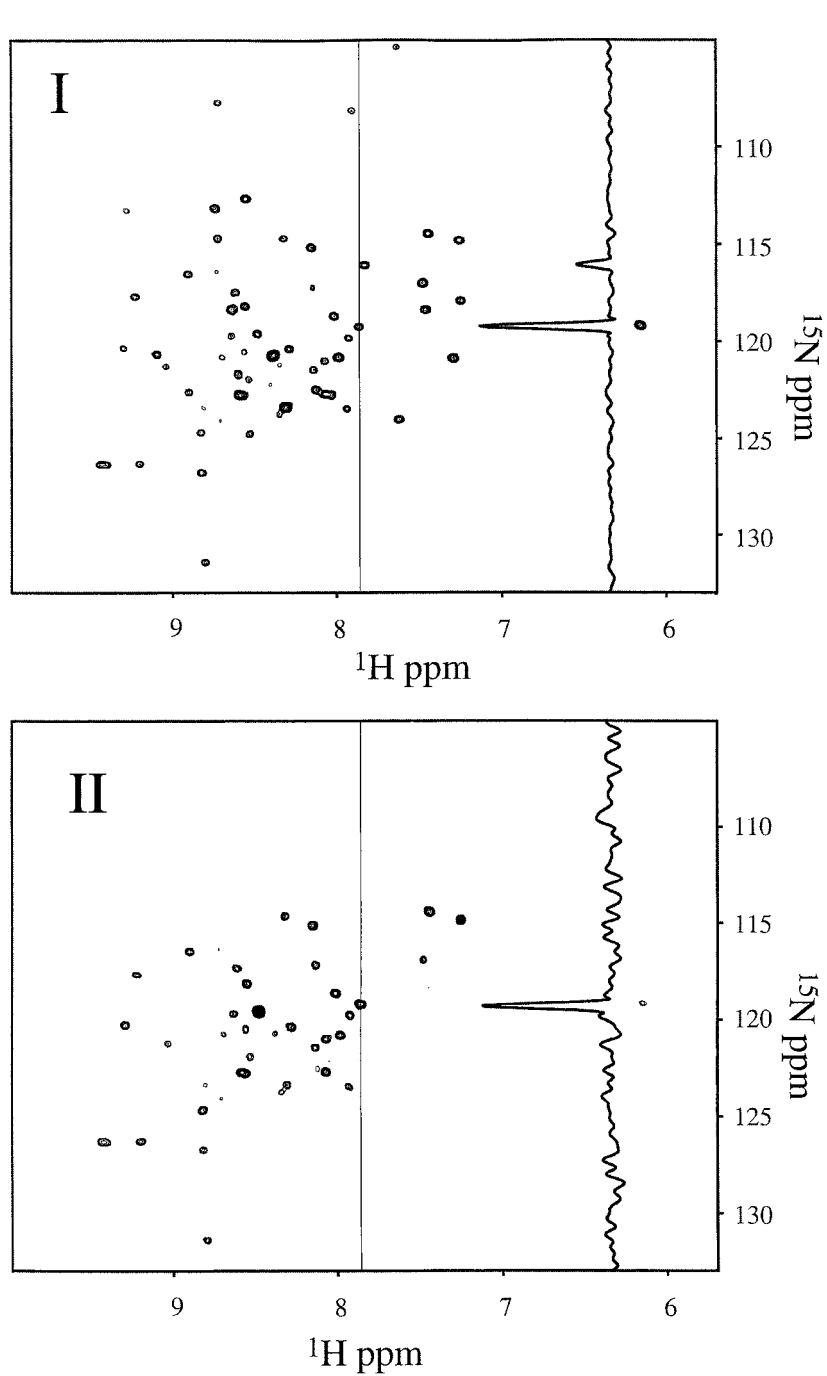
Figure 3. Representative spectra obtained with the sequence of Figure 1 at 600 MHz and 303 K to measure DD/DD cross-correlation rates in a sample of ^{13}C, ^{15}N- labeled human ubiquitin. The relaxation period T was set to 43 ms. The number of scans was 256 for experiment I and 768 for experiment II, resulting in a total acquisition time of 44 h. The representative vertical cross-sections shown correspond to Lysine 29. The peak heights provide information on the correlated motions of the two NH^N vectors of Lysine 29 and Isoleucine 30.

coherences. For this purpose, the pulse sequence has to be slightly modified: instead of removing the pulse marked by an asterisk in figure 1 in alternating scans, one must shift its phase by 90°. Note that since the phase of the receiver needs to be inverted on alternate scans in order to detect the double quantum coherences the unwanted pathway depicted in figure 1 is still suppressed. We shall refer to these experiments as I″ and II″. In this case however the rates R_1 and R_2 are no longer distinguishable from R_6 and R_7, and the measurements give

$$\frac{< 8N_+H_z^N N_+H_z^N >_{II''}(T)}{< 2N_+N_+ >_{I''}(T)} =$$
$$\tanh\left[(R_1 + R_2 + R_6 + R_7)T\right]. \tag{5}$$

Note that R_1 is the dominant term in both Equations (4) and (5) and that all rates in these equations depend on the same dihedral angles.

The CSA/CSA cross-correlation rate R_3 is indistinguishable from R_4 and R_5, hence

$$\frac{< 2N_xN_x >_{II'}(T)}{< 2N_yN_y >_{I'}(T)} = \tanh\left[(R_3 + R_4 + R_5)T\right]. \tag{6}$$

Results

The experiments of Figure 1 have been applied to a sample of ^{15}N/^{13}C labeled human ubiquitin that was obtained commercially (VLI). The protein was dissolved in 200 μl of 10% D$_2$O/90% H$_2$O with an acetate buffer at pH 4.5 to a concentration of 1.5 mM in a Shigemi tube. NMR data were acquired at 30 °C with a Bruker DMX-600 spectrometer equipped with a triple resonance TBI probe with triple axes gradients. The 2D spectra were acquired in an interleaved manner, with 256 scans for the reference experiment I and 768 scans for experiment II, using a relaxation delay of 1.4 s between subsequent scans. The spectral width was 14 ppm in the proton and 30 ppm in the nitrogen dimension. A total of 50 complex points was acquired in the indirect dimension. The experiments have been performed once for a relaxation delay $T = 21.5$ ms and twice with $T = 43$ ms. The relaxation period is chosen so that $T = 2n/^1J_{NH}$, with integer n, in order to minimize errors that might be caused by differential relaxation of in- and anti-phase operators (Meersman and Bodenhausen, 1995). In Figure 3 representative spectra obtained at $T = 43$ ms are shown. The cross-correlation rates were obtained from the intensity ratio of two experiments using Equation (4), averaged over

values obtained from different experiments. In Figure 4 the measured rates are plotted against the angle $\Theta^{NH,NH}$ between the NH^N bond vectors of successive residues, taken from X-ray (Vijay-Kumar et al., 1987) and NMR (Cornilescu et al., 1998) structures. When the measurements are plotted against the angles from the NMR structure there is less scatter. This suggests that the rates may be sensitive to the differences between structures determined in solution and in the crystalline phase. The curves in Figure 4 show the theoretical values for the NH^N/NH^N cross-correlation rate calculated for a molecule with a correlation time τ_c of 3.8 ns, without internal motion and assuming isotropic rotational diffusion

$$R_{NH,NH}^{rigid} = \left(\frac{\mu_0\hbar\gamma_H\gamma_N}{4\pi r_{NH}^3}\right)^2 P_2(\cos\Theta^{NH,NH})\frac{2\tau_c}{5}, \tag{7}$$

where P_2 is the second-order Legendre polynomial and the other symbols have their usual meaning. The gray circles represent the theoretical rates including the effects of R_2 and σ_{HH}. In Figure 5, the results are shown for an experiment where only DQ coherences are detected where the rates are insensitive to σ_{HH}.

We have also measured the CSA/CSA cross-correlation rates. The theoretical values for a rigid molecule that is tumbling isotropically can be readily predicted if we assume that the two CSA tensors have cylindrical symmetry

$$R_{N,N}^{rigid} = \left(\frac{2\gamma_N B_0\Delta\sigma}{3}\right)^2 P_2(\cos\Theta^{N,N})\frac{2\tau_c}{5}. \tag{8}$$

The experimental results are shown in Figure 6. For the theoretical curve the ^{15}N CSA tensors were assumed to be uniform for all amino acids, with an anisotropy $\Delta\sigma$ of 170 ppm and a principal axis rotated in the peptide plane through an angle of 20° away from the NH^N dipolar vector toward the carbonyl group (Tjandra et al., 1996). In Figure 7, the CSA/CSA rates are plotted against the DD/DD rates. Clearly, the fragments with angles $\Theta^{NH,NH}$ smaller and larger than 90° can be distinguished. These measurements can thus alleviate the ambiguity in the results of Figures 4 and 5.

Assuming planar geometry of the peptide bond, the angle $\Theta^{NH,NH}$ can be related to the dihedral angles ϕ and ψ defined in accordance to Ramanchandran's conventions, using standard bond angles as indicated in Figure 8:

$$\cos\Theta^{NH,NH} = 0.097 + 0.37\cos\psi + 0.47\cos\phi$$
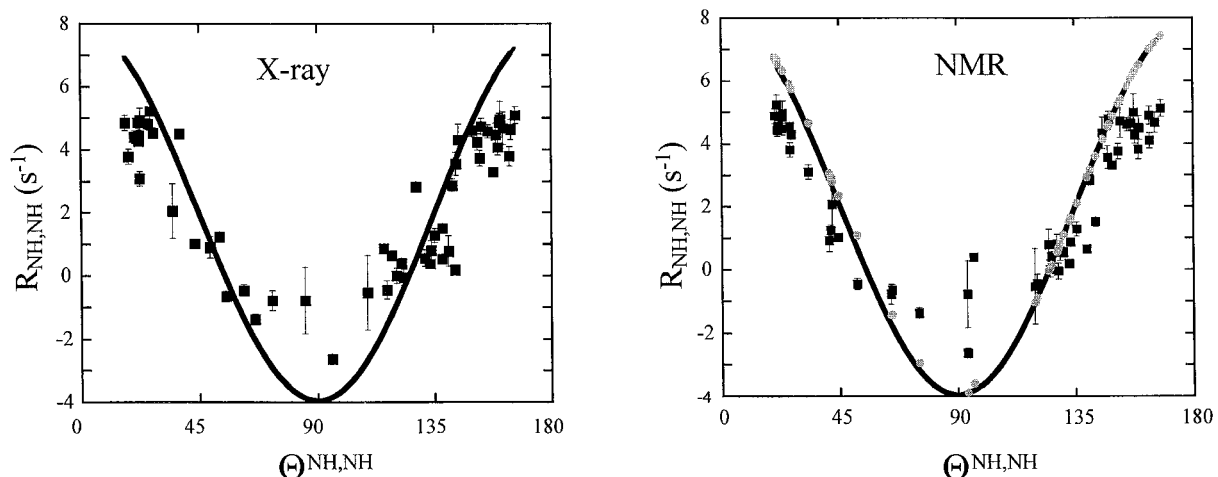$$-0.26\cos\psi\cos\phi + 0.72\sin\psi\sin\phi. \tag{9}$$

Figure 4. Experimental DD/DD cross-correlation rates, measured with the sequence of Figure 1 detecting both ZQ and DQ coherences plotted as a function of the angle $\Theta^{NH,NH}$ between NH^N vectors of successive residues a taken from the X-ray (left) and the NMR (right) structures. The solid lines represent the theoretical rates for a rigid molecule with an isotropic correlation time of 3.8 ns. The gray dots on the right represent the theoretical values for a rigid molecule including all contributions to the rates of Equation (4).
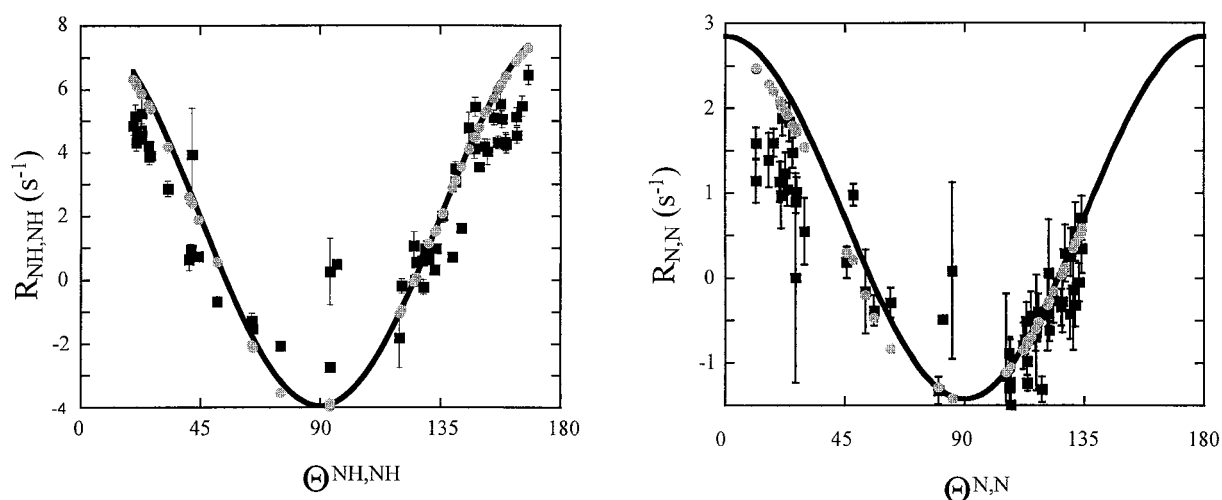
Figure 5. Same as Figure 4, except that only the DQ coherences have been detected and only the NMR structure has been used to obtain the angle $\Theta^{NH,NH}$. The gray dots include all rates of Equation 5.

Figure 6. Experimental CSA/CSA cross correlation rates plotted against the angle $\Theta^{N,N}$ between the unique axes of the CSA tensors estimated from the NMR structure. Each CSA tensor was assumed to be axially symmetric, with an anisotropy of 170 ppm and a symmetry axis tilted in the peptide plane by 20° from the NH^N vector toward the carbonyl atom. The gray dots include all rates of Equation 6.

A similar relation can be derived for the angle $\Theta^{N,N}$ between the unique axes of the two nitrogen CSA tensors:

$$\cos\Theta^{N,N} = 0.22 + 0.41\cos\psi + 0.50\cos\phi$$
$$-0.14\cos\psi\cos\phi + 0.39\sin\psi\sin\phi. \tag{10}$$

Figure 8 shows how the DD/DD and CSA/CSA rates depend on the dihedral angles ϕ and ψ. Clearly, many ambiguities can be resolved if the rates are compared to each other.

Discussion

If the global tumbling is isotropic, the discrepancies between the experimental and expected rates shown in Figures 4 and 5 can be ascribed to local motion. We may define a *heuristic order parameter* in the following manner

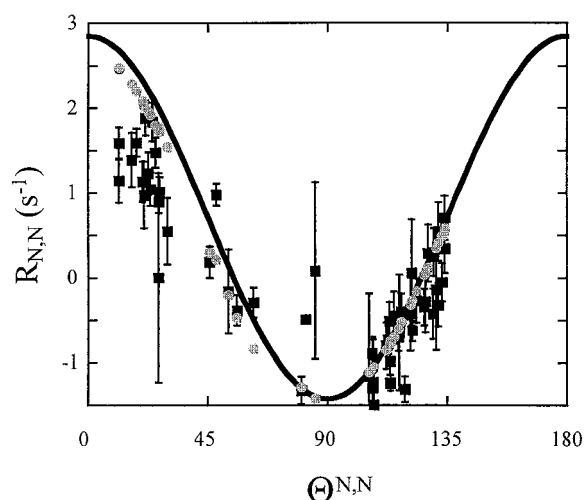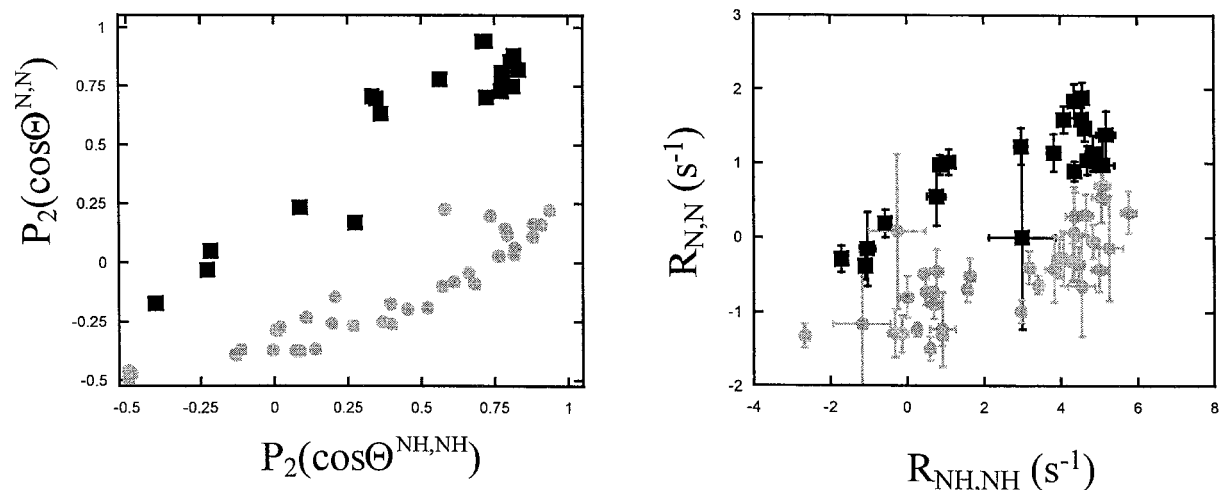*Figure 7.* Correlation of NH^N/NH^N (DD/DD) against N/N (CSA/CSA) cross-correlation rates. The theoretical values derived from the NMR structure are plotted on the left, while the experimental results are shown on the right. The black squares correspond to angles $0° < \Theta^{NH,NH} < 90°$, while the gray circles stand for angles $90° < \Theta^{NH,NH} < 180°$.

$$S^{2\,(heur)}_{NH,NH} = \frac{R^{exp}_{NH,NH}}{R^{rigid}_{NH,NH}}, \tag{11}$$

where $R^{exp}_{NH,NH}$ is the measured rate and $R^{rigid}_{NH,NH}$ the theoretical rate for a rigid molecule as defined in Equation 7. In Figure 9 the order parameter $S^{2\,(heur)}_{NH,NH}$ as defined in Equation 11 obtained with the experiments to measure the NH^N/NH^N cross-correlation rate is plotted against the residue number (we have omitted order parameters which, as a result of a small value of the denominator in Equation 11, have an error larger than 0.3). The values of the order parameter S^2_{NH} obtained by Tjandra et al. from the single quantum NH^N dipolar auto relaxation rates (Tjandra et al., 1995) are shown for comparison. It can be seen that the order parameters deviate considerably. In general the order parameters from the MQ cross-correlation are smaller than those obtained from SQ auto-correlation. Of course the order parameters need not be identical. A deeper analysis of the results needs to be performed in order to explain the differences.

It is instructive to reexamine the model-free formalism (Lipari and Szabo, 1982) in order to analyze our results. The DD/DD (or CSA/CSA) cross-correlation rate is determined by the spectral density

$$J^{u,v}(\omega) = 2 \int_0^\infty C^{u,v}(t) \cos \omega t \, dt \tag{12}$$

at zero frequency, i.e. $J^{u,v}(0) = 2 \int_0^\infty C^{u,v}(t) \, dt$, in which $C^{u,v}(t)$ is the correlation function and the indices u and v stand for different DD (or CSA) in-

teractions. For isotropic global motion, assuming that global and internal motions are independent, the total correlation function can be factored as:

$$C^{u,v}_{tot}(t) = C_{glob}(t)C^{u,v}_{int}(t) \tag{13}$$

with the correlation function for the global motion

$$C_{glob}(t) = \frac{1}{5}e^{-t/\tau_c} \tag{14}$$

and the internal correlation function

$$C^{u,v}_{int}(t) = < P_2[\mu^u(0) \cdot \mu^v(t)] > . \tag{15}$$

The unit vectors μ^u and μ^v describe the orientation of the interactions in a molecule-fixed reference frame. First we consider the case in which both interactions are associated with a fragment where the relative orientation $\Theta^{u,v}$ of the two interactions is fixed. For cross correlated interactions, the initial value of the internal correlation function is then given by

$$C^{u,v}_{int}(0) = P_2(\cos \Theta^{u,v}). \tag{16}$$

Using the addition theorem for spherical harmonics, Equation 15 can be written as:

$$C^{u,v}_{int}(t) = \frac{4\pi}{5} \sum_{m=-2}^{2} < Y^u_{2m}{}^*(0)Y^v_{2m}(t) > . \tag{17}$$

Under the influence of internal motions, the correlation function decays and its limiting value for $t \to \infty$ is defined as the *cross-correlation order parameter* (Früh, 2002):

$$S^2_{u,v} \equiv C^{u,v}_{int}(\infty) = \frac{4\pi}{5} \sum_{m=-2}^{2} < Y^u_{2m}{}^* >< Y^v_{2m} > . \tag{18}$$
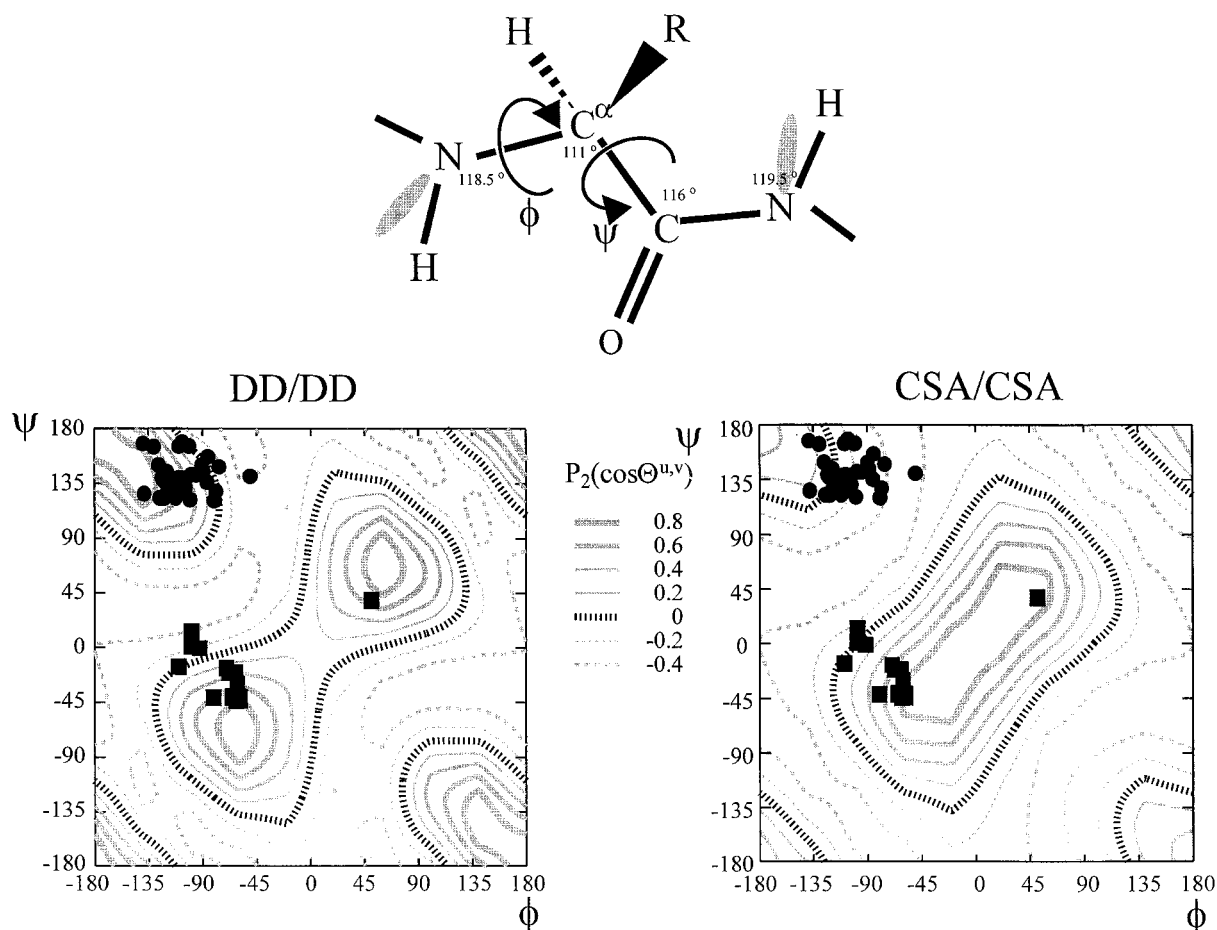
Figure 8. Fragment of a protein backbone with plots of the Legendre polynomials that determine the NH^N/NH^N (DD/DD) and N/N (CSA/CSA) cross-correlation rates for rigid molecules, shown as a function of the dihedral angles ϕ and ψ defined according to Ramanchandran's conventions. The sketch correspond to $\phi = \psi = 180°$. The black squares and circles correspond to the ϕ- and ψ-angles from the NMR structure of ubiquitin. For the clusters centered on $\phi = -90°$ and $\psi = -20°$, where residues located in α helices can be found, $\Theta^{NH,NH}$ and $\Theta^{N,N}$ are similar and the $P_2(\cos \Theta^{u,v})$ that determine the DD/DD and CSA/CSA rates are also comparable. For the cluster centered on $\phi = -100°$ and $\psi = +140°$, where residues in β sheets appear, the functions $P_2(\cos \Theta^{NH,NH})$ are mostly positive and $P_2(\cos \Theta^{N,N})$ mostly negative, thus allowing an easy distinction between the two clusters.

The ensemble averages $< Y_{2m}^{u}{}^{*} >$ and $< Y_{2m}^{v} >$ of the spherical harmonic functions depend on various internal motions that affect the orientations Ω_u and Ω_v of the interactions u and v with respect to a molecule-fixed frame. They can be described by appropriate orientational probability distribution functions $p(\Omega_u)$ and $p(\Omega_v)$ governed by internal motions.

$$C_{int}^{u,v}(\infty) = \tag{19}$$

$$\iint P_2[\cos \Theta^{u,v}(\Omega_u, \Omega_v)] p(\Omega_u) p(\Omega_v) d\Omega_u d\Omega_v,$$

where the relative angle $\Theta^{u,v}(\Omega_u, \Omega_v)$ is determined by the absolute orientations Ω_u and Ω_v. In the 'model-free' approach proposed by Lipari and Szabo (Lipari

and Szabo, 1982), the probability distribution functions are not evaluated explicitly in terms of a specific model for internal motion. Instead, the internal correlation function is defined to feature an exponential decay from its initial value to an asymptotic value:

$$C_{int}^{u,v}(t) = C_{int}^{u,v}(\infty) - [C_{int}^{u,v}(\infty) - C_{int}^{u,v}(0)]e^{-t/\tau_{int}} =$$

$$S_{u,v}^2 - [S_{u,v}^2 - P_2(\cos \Theta^{u,v})]e^{-t/\tau_{int}}, \tag{20}$$

where τ_{int} is the correlation time of the internal motion. This leads to a spectral density

$$J^{u,v}(\omega) = \frac{2}{5}\left(\frac{S_{u,v}^2 \tau_c}{1 + (\omega\tau_c)^2} + \frac{[P_2(\cos \Theta^{u,v}) - S_{u,v}^2]\tau}{1 + (\omega\tau)^2} \right), \tag{21}$$

Figure 9. Ratio $S^{2\,(heur)}_{NH,NH}$ as defined in Equation 11 between measured rates and the theoretical values for a rigid molecule for DD/DD 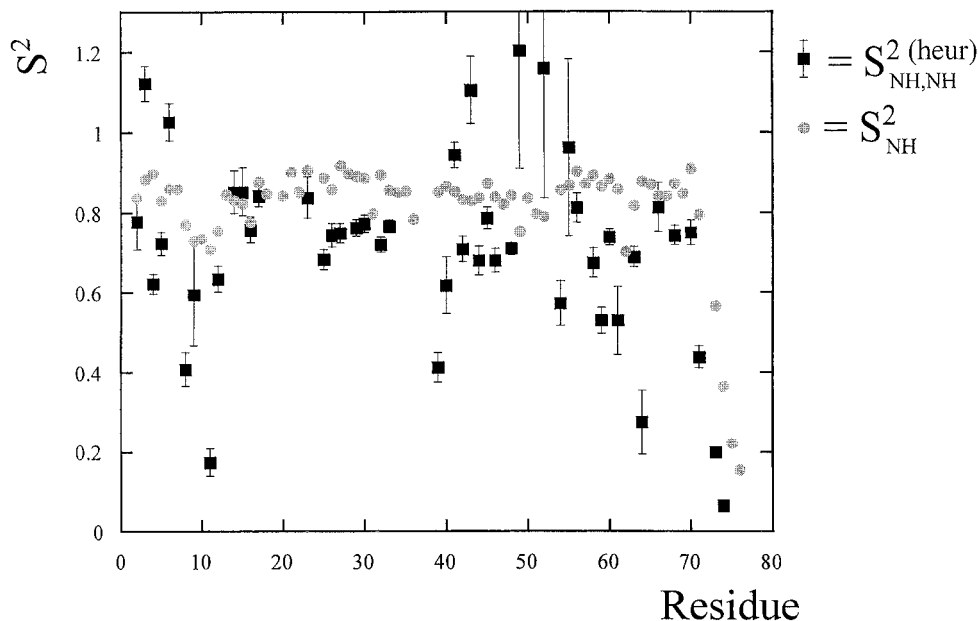cross-correlation between two successive NH^N vectors using the NMR structure for reference (black squares). The rates are averages of those presented in Figures 4 and 5. Rates with errors larger than 0.3 are not shown. Also shown are the values of the Lipari-Szabo order parameter S^2_u obtained from single quantum relaxation measurements on amide nitrogen nuclei (gray circles).

where $\tau^{-1} = \tau_c^{-1} + \tau_{int}^{-1}$ so that $\tau \approx \tau_{int}$ if $\tau_{int} \ll \tau_c$, i.e., if the internal motions are fast. Note that the effect of internal motions that are slower than global tumbling will be masked by the exponential decay of the global correlation function, since $\tau \approx \tau_c$ if $\tau_{int} \gg \tau_c$ in which case $J^{u,v}(\omega) = \frac{2}{5} P_2(\cos \Theta^{u,v}) \tau_c / (1 + \omega^2 \tau_c^2)$ regardless of $S^2_{u,v}$. Hence the ∞ in Equation 18 may be interpreted as only a few times the global correlation time τ_c. For rigid or slow-moving fragments the relaxation rates depend only on the correlation time τ_c of the global motion and the relative orientation $\Theta^{u,v}$ of the spin interactions. If on the other hand, the internal motions of the fragments are much faster than the global motion, the rates depend on the amplitude of these motions through the cross-correlation order parameter $S^2_{u,v}$ defined in Equation 18, provided the fast internal motions are indeed truly independent of the global motion. In the case that slow conformational exchange influences the fast internal motion it is better to speak of an average order parameter. The previous equations have to be averaged over the different conformations with suitable weights. For example, Equation 20 becomes:

$$C_{int}^{u,v}(t) = \overline{S^2_{u,v} - [S^2_{u,v} - P_2(\cos \Theta^{u,v})]e^{-t/\tau_{int}}}. \quad (22)$$

The theory presented above is also applicable for auto-correlation rates, provided one replaces the index v by u and sets $\Theta^{u,u}$ to zero.

In the case of DD/DD cross-correlation between two successive NH^N interactions the rigid body approximation is not likely to be fulfilled, hence one cannot speak of a fixed angle $\Theta^{u,v}$ between the two interactions. In a first approximation we assume that there is no correlation between the local motions of successive NH^N vectors. In this case the internal cross-correlation function is time independent:

$$C_{int}^{u,v}(t) = C_{int}^{u,v}(\infty) \equiv S^2_{u,v} =$$

$$\frac{4\pi}{5} \sum_{m=-2}^{2} < Y^u_{2m}{}^* > < Y^v_{2m} > . \quad (23)$$

This equation is identical to Equation 18, except that only motions that are on the order of or faster than the global correlation time must be taken into account for the averaging in Equation 18, while motions on *all time scales* are important in Equation 23. The effect of slow uncorrelated motions is thus fundamentally different compared to the effect of two interactions that are rigidly fixed with respect to each other (or to the effect of auto-correlated relaxation) as expressed in Equation 22. While in Equation 22 the slow inter-

nal motions only indirectly affect the relaxation rate if they influence the fast motions, in Equation 23 the order parameter is directly affected by the amplitude of the slow motion and has exactly the same effect as fast motions.

We now consider the effect of internal motions for the specific case of DD/DD cross-correlated relaxation involving two NH^N dipolar interactions of successive residues. Clearly the rapid fluctuations of the orientations of the peptide planes in which each of these interactions are located contributes to a decrease of the order parameter observed in cross correlated relaxation. These fast internal motions are the same as those which are reflected in the auto-correlated single quantum NH^N dipolar relaxation rate. It is not possible to relate the order parameters S_u^2 and S_v^2 derived from the single quantum relaxation rates to the order parameter $S_{u,v}^2$ of the cross-correlation rate without precise knowledge of the angular probability distributions $p(\Omega_u)$ and $p(\Omega_v)$ of the individual interactions. However, if each angular probability distribution is approximated by a function that does not depend on the azimuthal angle, i.e., if the fluctuations of each NH^N interaction are axially symmetric with respect to the average NH^N orientation (the hypothesis of 'axial symmetry'), the SQ order parameter is given by:

$$S_u^2 = < P_2(\cos \Theta^u) >^2, \qquad (24)$$

where Θ^u is the angle between the instantaneous and the average positions of the vector $\vec{r_u}$ (NH^N). With the same hypothesis, the cross-correlated order parameter can be expressed as

$$S_{u,v}^2 = S_u S_v P_2(\cos \Theta^{u,v}), \qquad (25)$$

where $S_u = < P_2(\cos \Theta^u) >$ and $\Theta^{u,v}$ is the angle between the average orientations of the interactions u and v. The cross-correlation order parameter therefore contains both structural and dynamic information. In order to separate these two contributions one can define a dynamic order parameter as:

$$S_{u,v}^{2\,(dyn)} = S_{u,v}^2 / P_2(\cos \Theta^{u,v}) = S_u S_v, \qquad (26)$$

i.e., the order parameter of Equation 25 is divided by the second-order Legendre polynomial which corresponds to the order parameter for a rigid molecule. This definition is consistent with the heuristic order parameter of Equation 11 used in Figure 9.

Recent studies of dynamics from residual dipolar couplings (RDCs) and molecular dynamics calculations (Meiler et al., 2001) indicate that the assumption of axial symmetry of the individual NH^N fluctuations is valid for most residues of ubiquitin. However considerable motional asymmetries (and thus violations of Equation 25) are expected for residues in the loop regions (Thr7 to Lys11, Gly35, Ile36, Gly47, Gly53, Arg54) and in the flexible C-terminus. In the results shown in Figure 9, the nature of the fluctuations of NH^N vectors within a peptide plane is apparent. For the order parameters derived from the NH^N/NH^N cross-correlation rates, the residues with asymmetric NH^N motions show large deviations from the average. However, the order parameters estimated from the cross-correlation rate are on average lower than would be expected from an estimate based on auto-correlated relaxation, even excluding these residues. If the assumption of axial symmetry of the fast motions is verified for most residues, this discrepancy must be due to motions that are slower than the global correlation time. In Figure 10 the effect of slow motions on the cross-correlated order parameter is illustrated in the case where both residues exhibit motions that are axially symmetric. The internal correlation function is plotted for two interactions u and v, along with the resulting total correlation function. Two models are assumed, model A with internal motions that are ten times faster than the global correlation time, $\tau_{int}^{fast} = \tau_c/10$, model B with additional internal motions that are ten times slower than the global correlation time, $\tau_{int}^{slow} = 10\tau_c$. The internal correlation function for model A can be obtained from Equation 20 (Lipari and Szabo, 1982).

For model B the internal auto-correlation function is given by (Clore et al., 1990)

$$C_{int}^{u,u} = S_u^{2\,(fast)} \times S_u^{2\,(slow)} + [1 - S_u^{2(fast)}]e^{-t/\tau_{int}^{fast}}$$
$$+ [S_u^{2(fast)} - S_u^{2(fast)} \times S_u^{2(slow)}]e^{-t/\tau_{int}^{slow}}. \qquad (27)$$

In the model calculation of Figure 10, the order parameters corresponding to the fast internal motion are assumed to be (a) $S_u^{2\,(fast)} = 0.9$ and (b) $S_v^{2\,(fast)} = 0.8$, respectively, while the slow internal motion further decreases the resulting internal order parameters to (a) $S_u^{2\,(fast)} \times S_u^{2\,(slow)} = 0.7$ and (b) $S_v^{2\,(fast)} \times S_v^{2\,(slow)} = 0.6$. At the right of the plots the spectral densities $J(0)$ as defined in Equation 12, i.e., the integrals over the total correlation functions, are given for the different models (normalized to the spectral density for global motions in the absence of internal mobility). The values of $J(0)$ are almost identical for both models in the case of the auto-correlated correlation functions (a) and (b), indicating that slow motions hardly affect the outcome.
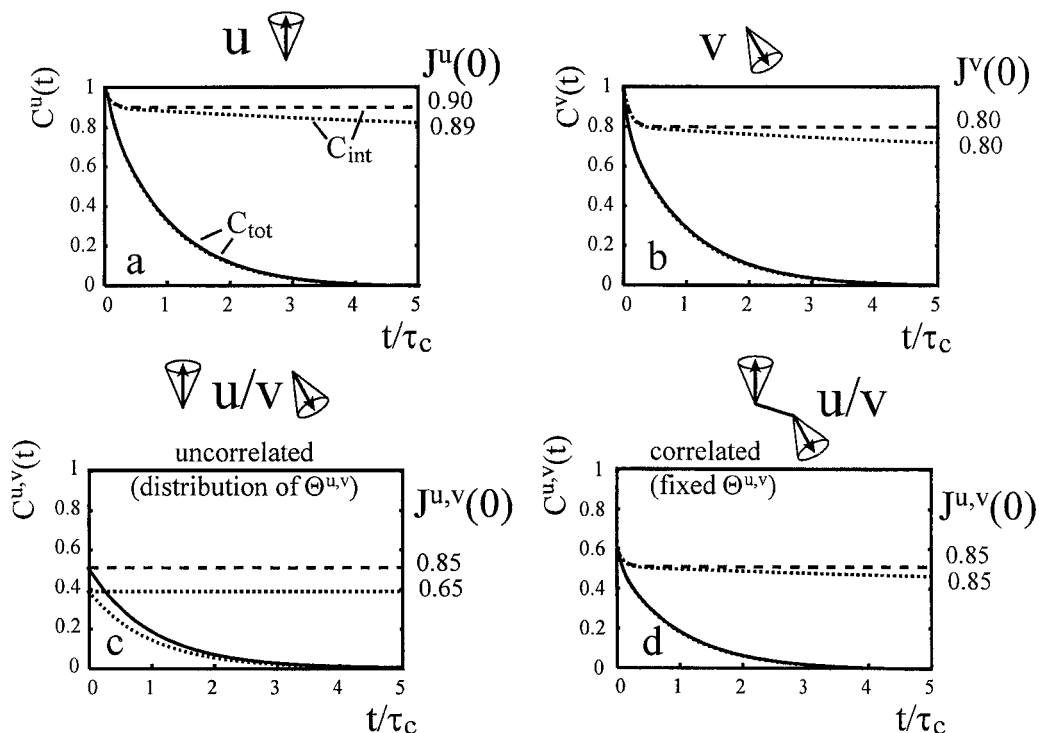
Figure 10. Internal correlation functions for two interactions that exhibit azimuthal symmetric motion. In (a) and (b) the auto-correlated correlation functions are displayed, in (c) the cross-correlation function is shown for uncorrelated modulations of the two interactions and in (d) for two interactions with orientations that are fixed with respect to each other. The correlation functions are plotted for two different cases. In the first case (dashed lines) only very fast internal motions are considered with a local correlation time $\tau_{int}^{fast} = \tau_c/10$. The second case (dotted lines) includes an additional slow internal motion with a correlation time $\tau_{int}^{slow} = \tau_c \times 10$. In fragment u the order parameters are $S_u^{2\,(fast)} = 0.9$ and $S_u^{2\,(fast)} \times S_u^{2\,(slow)} = 0.7$. The corresponding values for fragment v are $S_v^{2\,(fast)} = 0.8$ and $S_v^{2\,(fast)} \times S_v^{2\,(slow)} = 0.6$. The cross-correlated order parameters as obtained by Equation 26 are $S_{u,v}^{2\,(fast)} = 0.85$ and $S_{u,v}^{2\,(fast)} \times S_{u,v}^{2\,(slow)} = 0.65$. In (a), (b) and (d) the spectral density $J(0)$ (numbers on the right of each figure) as defined in Equation 12 is essentially determined by the order parameter of the very fast internal motion alone, while in (c) both fast and slow internal motions are important, leading to a lower spectral density $J(0)$. The spectral densities are normalized to a rigid molecule. In each of the frames the total correlation function of Equation 13 is also plotted.

When the motions of u and v are completely uncorrelated the cross-correlated correlation function of Equation 23 with order parameters as defined in Equations 25 and 26 is affected by motions on *all time scales* (Figure 10c). Hence a clear difference can be seen between model A (only fast motions) and the model B (that also includes slow motions).

In the case where the interactions u and v are rigidly fixed with respect to each other so that $\Theta^{u,v}$ is time independent, Equation 20 has to be used to express the correlation function for the model A with only fast motions. For model B with additional slow motions Equation 27 has to be slightly adapted to express the cross-correlated correlation function:

$$C_{int}^u = S_{u,v}^{2\,(fast)} \times S_{u,v}^{2\,(slow)} + [P_2(\cos \Theta^{u,v})$$
$$-S_{u,v}^{2(fast)}]e^{-t/\tau_{int}^{fast}} + [S_{u,v}^{2(fast)} - S_{u,v}^{2(fast)} \tag{28}$$
$$\times S_{u,v}^{2(slow)}]e^{-t/\tau_{int}^{slow}}.$$

As in the case of the auto-correlated relaxation only very fast motions significantly affect the spectral density (Figure 10d). Hence, a measurable difference can be seen for the cross-correlated spectral densities when slow internal motions are present between the two cases of correlated and uncorrelated internal motions. Note that in Figures 10a, 10b and 10d it has been assumed that the internal motion is uniform for all conformations, that is to say the averaging of Equation 22 has been neglected. The cross-correlated order parameters have been taken from Equation 26. In reality the cross-correlated order parameter is given by:

$$S_{u,v}^{2\,(dyn)} = \overline{S_u S_v}. \tag{29}$$

However this might only lead to considerable differences when the auto-correlated order parameters vary significantly over the different conformations in a correlated way.

In reality the motions are likely to be much more complex than in the two simple models we have presented. The motions could be partly correlated (or anti-correlated). The decay of the correlation functions would probably lie between those shown in Figures 10c and 10d. Efforts are under way in our laboratory to refine the theory in order to account for all possible kinds of motions.

It is not possible to draw definitive conclusions about the exact nature of the motions from these measurements. Based on the average value of the cross-correlated order parameter of $< S_{u,v}^{2\,(heur)} > = 0.75$ (an average that excludes the outliers and terminal residues) compared to $< S_u^2 > = 0.85$ for the average auto-correlated order parameter, we conclude that the amplitudes of the slow motions that cannot be detected by traditional single quantum methods must be considerable. It is difficult to make statements about the timescale of these motions, although they must be outside the range of very fast motions that can be detected by measurements of the auto-correlated relaxation rates. This seems in agreement with recent studies based on residual dipolar couplings (Peti et al., 2002; Tolman, 2002).

Conclusions

In this paper we have presented new methods to measure relaxation rates of two-spin coherences involving two amide nitrogen nuclei of successive amino-acids in proteins and peptides. These rates are sensitive to structural and dynamic parameters. In contrast to auto-correlation rates and short-range cross-correlation rates (such as the DD/CSA rate between NH^N and N of the *same* residue), these rates are sensitive to local motions on *all* time scales and not only to motions that are faster than or comparable to global tumbling. The new experiments are useful to complement information that can be obtained from auto-correlation rates, which are mostly sensitive to fast internal motions on time-scales $\tau_{int} < \tau_c$. They can also complement slow time-scale exchange experiments. The NH^N/NH^N cross-correlation rates that are obtained in a sample of ^{15}N,^{13}C-labeled ubiquitin

strongly suggest the presence of internal motions that are slower than the global correlation time.

Acknowledgements

Appendix A: Effects of H^N(i)-H^N(i+1) cross-relaxation

In order to consider the influence of cross-relaxation (Overhauser effect) between two amide protons on the relaxation of a two-spin coherence between the amide nitrogens of successive residues, it is useful to expand the density operator in a basis of single transition operators.

$$b_{++} = \begin{pmatrix} < 2N_+ H_\alpha^N N_+ H_\alpha^N > \\ < 2N_+ H_\alpha^N N_+ H_\beta^N > \\ < 2N_+ H_\beta^N N_+ H_\alpha^N > \\ < 2N_+ H_\beta^N N_+ H_\beta^N > \end{pmatrix}$$

$$b_{+-} = \begin{pmatrix} < 2N_+ H_\alpha^N N_- H_\alpha^N > \\ < 2N_+ H_\alpha^N N_- H_\beta^N > \\ < 2N_+ H_\beta^N N_- H_\alpha^N > \\ < 2N_+ H_\beta^N N_- H_\beta^N > \end{pmatrix}. \tag{A1}$$

One can describe the evolution of DQ and ZQ coherences independently:

$$\frac{db_{++}}{dt} = -\mathcal{L}_{++} b_{++} \tag{A2}$$

and

$$\frac{db_{+-}}{dt} = -\mathcal{L}_{+-} b_{+-}, \tag{A3}$$

where $\mathcal{L}_{++}$ is the Liouvillian for the DQ coherence

$$\mathcal{L}_{++} = \begin{pmatrix} R_{av} + R_{++}^{\alpha\alpha} - W_{\alpha\alpha,\alpha\alpha} & -W_{\alpha\alpha,\alpha\beta} \\ -W_{\alpha\alpha,\alpha\beta} & R_{av} + R_{++}^{\alpha\beta} - W_{\alpha\beta,\alpha\beta} \\ -W_{\alpha\alpha,\beta\alpha} & -W_{\alpha\beta,\beta\alpha} \\ -W_{\alpha\alpha,\beta\beta} & -W_{\alpha\beta,\beta\beta} \end{pmatrix}$$

$$\begin{pmatrix} -W_{\alpha\alpha,\beta\alpha} & -W_{\alpha\alpha,\beta\beta} \\ -W_{\alpha\beta,\beta\alpha} & -W_{\alpha\beta,\beta\beta} \\ R_{av} + R_{++}^{\beta\alpha} - W_{\beta\alpha,\beta\alpha} & -W_{\beta\alpha,\beta\beta} \\ -W_{\beta\alpha,\beta\beta} & R_{av} + R_{++}^{\beta\beta} - W_{\beta\beta,\beta\beta} \end{pmatrix} \quad \text{(A4)}$$

$$+i \begin{pmatrix} \Omega_{++} + \pi J_{++} & 0 & 0 & 0 \\ 0 & \Omega_{++} + \pi J_{+-} & 0 & 0 \\ 0 & 0 & \Omega_{++} - \pi J_{+-} & 0 \\ 0 & 0 & 0 & \Omega_{++} - \pi J_{++} \end{pmatrix}.$$

The rates $R_{++}^{\gamma\gamma}$ correspond to differential line broadening and narrowing so that $R_{++}^{\alpha\alpha} + R_{++}^{\alpha\beta} + R_{++}^{\beta\alpha} + R_{++}^{\beta\beta} + R_{+-}^{\alpha\alpha} + R_{+-}^{\alpha\beta} + R_{+-}^{\beta\alpha} + R_{+-}^{\beta\beta} = 0$. These rates depend on the different cross-correlation rates of Table 1 as indicated in Table A.1. The average rate R_{av} is common to all transitions and is mainly determined by auto-correlation effects. J_{++} and J_{+-} are the sum and difference between the one-bond scalar couplings $^1J_{NH}(i) \pm^1 J_{NH}(i+1)$ and Ω_{++} is the sum of the chemical shifts of the two nitrogens. The diagonal elements of the W matrix are defined so that the sum over the rows or columns of W vanishes (e.g., $W_{\alpha\alpha,\alpha\alpha} = -(W_{\alpha\alpha,\alpha\beta} + W_{\alpha\alpha,\beta\alpha} + W_{\alpha\alpha,\beta\beta})$). The terms $W_{\alpha\alpha,\alpha\beta}$, $W_{\alpha\alpha,\beta\alpha}$, $W_{\alpha\beta,\beta\beta}$ and $W_{\beta\alpha,\beta\beta}$ represent rates of single spin-flips of one of the two H^N protons and are mainly due to DD interactions with other protons and to chemical exchange. $W_{\alpha\beta,\beta\alpha}$ gives the rate of a flip-flop process and is given by:

$$W_{\alpha\beta,\beta\alpha} = \left(\frac{\mu_0 \hbar \gamma_H^2}{4\pi r_{HH}^3}\right)^2 \times$$

$$< [\frac{1}{2} H_-^N H_+^N, [\frac{1}{2} H_+^N H_-^N, 2N_+ H_\beta^N N_+ H_\alpha^N]]|$$
$$2N_+ H_\alpha N_+ H_\beta > J(0) \quad \text{(A5)}$$

$$= \left(\frac{\mu_0 \hbar \gamma_H^2}{4\pi r_{HH}^3}\right)^2 \times \frac{1}{4} \times J(0) = \sigma_{HH},$$

where σ_{HH} is identical to the NOE-rate between the two amide protons in the slow tumbling limit. The rate $W_{\alpha\alpha,\beta\beta}$ correspond to flop-flop processes, which will be neglected in the further discussion, since they are proportional to the spectral density $J(2\omega_H)$ and therefore expected to be very small in macromolecules.

Also the $H^N H^N / H^N$ (DD/CSA) cross-correlation rate, which is proportional to the spectral density $J(\omega_H)$ will be neglected. In this case $W_{\alpha\alpha,\alpha\beta} = W_{\beta\alpha,\beta\beta}$ and $W_{\alpha\alpha,\beta\alpha} = W_{\alpha\beta,\beta\beta}$.

The Liouvillian $\mathcal{L}_{+-}$ for the ZQ coherences is identical, except that the indices $++$ have to be changed to $+-$. The off-diagonal elements can be neglected when they are much smaller than the difference between the diagonal elements they connect (Redfield, 1965). Since the scalar couplings involved are large one can neglect all off-diagonal terms except $W_{\alpha\beta,\beta\alpha}$. This rate can only be neglected in the (unlikely) case that the scalar couplings $^1J_{NH}(i)$ and $^1J_{NH}(i+1)$ are very different from each other. In this case only the diagonal terms remain. One can then redefine R_{av} as (Chiarparin, 2000):

$$R'_{av} = R_{av} + W_{\alpha\alpha,\alpha\beta} + W_{\alpha\alpha,\beta\alpha} + \frac{1}{2}\sigma_{HH}. \quad \text{(A6)}$$

The real part of the Liouvillian then becomes:

$$R_{++} = \begin{pmatrix} R'_{av} + R_{++}^{\alpha\alpha} - \frac{1}{2}\sigma_{HH} & 0 \\ 0 & R'_{av} + R_{++}^{\alpha\beta} + \frac{1}{2}\sigma_{HH} \\ 0 & 0 \\ 0 & 0 \end{pmatrix}$$

$$\begin{pmatrix} 0 & 0 \\ 0 & 0 \\ R'_{av} + R_{++}^{\beta\alpha} + \frac{1}{2}\sigma_{HH} & 0 \\ 0 & R'_{av} + R_{++}^{\beta\beta} - \frac{1}{2}\sigma_{HH} \end{pmatrix} \quad \text{(A7)}$$

and likewise for R_{+-}. In the DQ space, the alternating signs $-$, $+$, $+$, $-$ of the σ_{HH} terms are reminiscent of the contributions of the rates R_1, R_2, R_6 and R_7. In the ZQ space only the rates R_6 and R_7 follow the same pattern whereas the contributions of the rates R_1 and R_2 to the relaxation of the four coherences have opposite signs. Since a two-spin coherence such as $2N_y N_y$ is a sum of DQ and ZQ coherences the net effect of σ_{HH} is similar to that of R_6 and R_7.

When the scalar couplings are similar (as is often the case for one-bond amide NH couplings) the effects are different for the ZQ and DQ coherences. For the ZQ coherences the secular approximation remains valid since the difference in precession frequencies of the coherences that are connected by $W_{\alpha\beta,\beta\alpha}$ is given by the sum of the scalar couplings $^1J_{NH}(i) + ^1J_{NH}(i+1)$. For the DQ coherences the situation is drastically different. To determine the effect of this term it suffices to consider the reduced subspace of Equation A4 describing the two central lines. One can redefine R_{av} as

Table A.1. Contribution of cross-correlation rates of Table 1 to the relaxation of single transition operators that describe individual components of the double- and zero-quantum multiplets

	$R^{\alpha\alpha}_{++}$	$R^{\alpha\beta}_{++}$	$R^{\beta\alpha}_{++}$	$R^{\beta\beta}_{++}$	$R^{\alpha\alpha}_{+-}$	$R^{\alpha\beta}_{+-}$	$R^{\beta\alpha}_{+-}$	$R^{\beta\beta}_{+-}$
$R_{1,2}$	+	−	−	+	−	+	+	−
$R_{3,4,5}$	+	+	+	+	−	−	−	−
$R_{6,7}$	+	−	−	+	+	−	−	+
$R_{8,9}$	+	+	−	−	+	+	−	−
$R_{10,11}$	+	−	+	−	+	−	+	−
$R_{12,13}$	+	+	−	−	−	−	+	+
$R_{14,15}$	+	−	+	−	−	+	−	+

$$R''_{av} = R_{av} + W_{\alpha\alpha,\alpha\beta} + W_{\alpha\alpha,\beta\alpha}. \tag{A8}$$

The Liouvillian in the reduced subspace then becomes:

$$\mathcal{L}^{red}_{++} = \begin{pmatrix} R''_{av} + R^{\alpha\beta}_{++} + \sigma_{HH} + i(\Omega_{++} + \pi J_{+-}) & -\sigma_{HH} \\ -\sigma_{HH} & R''_{av} + R^{\beta\alpha}_{++} + \sigma_{HH} + i(\Omega_{++} - \pi J_{+-}) \end{pmatrix}. \tag{A9}$$

Even if $J_{+-} = 0$, i.e., if the two inner lines in the doublet of doublets of the double quantum spectrum are exactly degenerate, the off-diagonal terms σ_{HH} still manifest themselves since the inherent line-widths of the two degenerate transitions can be unequal ($R^{\alpha\beta}_{++} \neq R^{\beta\alpha}_{++}$). In general Equation A9 must be diagonalized to obtain a complete description of the time evolution, but in actual fact the use of π-pulses allows one to interchange coherences at will, so that it is sufficient to focus on the zeroth order average Liouvillian. The π-pulse on the nitrogen nuclei causes an interchange of the +2 and −2 coherences, so that one also has to consider the complex conjugate of Equation A9. If we consider the pulse sequence of Figure 2, the zeroth order average Liouvillian is given by:

$$\mathcal{L}^{av,red}_{++} = \begin{pmatrix} R'''_{av} + \sigma_{HH} & -\sigma_{HH} \\ -\sigma_{HH} & R'''_{av} + \sigma_{HH} \end{pmatrix}, \tag{A10}$$

where $R'''_{av} = R''_{av} + \sum_{i=1}^{7} (\varepsilon^{\alpha\beta}_{++})_i R_i$ and where the summation runs over the first seven rates of Table 1 and $(\varepsilon^{\alpha\beta}_{++})_i$ can assume the values +1 or −1 depending on whether the rate gives a positive or negative contribution to the relaxation of the $2N_+ H^N_\alpha N_+ H^N_\beta$ coherence, as indicated in Table A.1. Since the pulse sequence is symmetric the calculation is exact up to second order (Ghose, 2000). The eigenvectors

in the subspace of Equation A10 are the sum and the difference of the double-quantum coherences $< 2N_+ H^N_\alpha N_+ H^N_\beta > \pm < 2N_+ H^N_\beta N_+ H^N_\alpha >$ and the diagonalized average Liouvillian is

$$\mathcal{L}^{av,red,diag}_{++} = \begin{pmatrix} R'''_{av} & 0 \\ 0 & R'''_{av} + 2\sigma_{HH} \end{pmatrix}. \tag{A11}$$

If the initial operator is given by $2N_y N_y$ then the initial state in the reduced subspace is described by the first eigenvector of Equation A11. Cross relaxation has therefore no influence on the evolution of the DQ coherences. By contrast, the σ_{HH} term appears on the diagonal of the zero-quantum Liouvillian $\mathcal{L}_{+-}$ while the off-diagonal terms must be dropped from $\mathcal{L}_{+-}$ due to the secular approximation ($\sigma_{HH} \ll {}^1 J_{NH}(i) + {}^1 J_{NH}(i+1)$) so that the sum and differences of the zero-quantum coherences $< 2N_+ H^N_\alpha N_- H^N_\beta > \pm < 2N_+ H^N_\beta N_- H^N_\alpha >$ are *not* eigenvectors of $\mathcal{L}_{+-}$. In the experiment we detect the operators $2N_y N_y$ and $8N_x H_z N_x H_z$, which are superpositions of ZQ and DQ coherences. The ratio between the expectation values of both operators is therefore given by:

$$\frac{< 8N_x H_z N_x H_z > (T)}{< 2N_y N_y > (T)} \tag{A12}$$

$$\approx \frac{\sinh[(R_1 + R_2 + \frac{1}{2}\sigma_{HH})T] + \sinh[(R_1 + R_2)T]}{\cosh[(R_1 + R_2 + \frac{1}{2}\sigma_{HH})T] + \cosh[(R_1 + R_2)T]}$$

$$\approx \tanh[(R_1 + R_2 + \frac{1}{4}\sigma_{HH})T].$$

This approximation is valid when $\sigma_{HH} T \ll 1$. The results of this calculation have been confirmed by numerical simulations over a wide range of realistic values for the different scalar couplings and cross-correlation rates.

References

Akke, M. and Palmer, A.G. (1996) *J. Am. Chem. Soc.*, **118**, 911–912.

Brutscher, B., Bremi, T., Skrynnikov, N., Brüschweiler, R. and Ernst, R.R. (1998) *J. Magn. Reson.*, **130**, 346–351.

Carlomagno, T., Maurer, M., Hennig, M. and Griesinger, C. (2000) *J. Am. Chem. Soc.*, **122**, 5105–5113.

Chiarparin, E. (2000) PhD thesis, University of Lausanne.

Chiarparin, E., Pelupessy, P., Ghose, R. and Bodenhausen, G. (1999) *J. Am. Chem. Soc.*, **121**, 6876–6883.

Chiarparin, E., Pelupessy, P., Ghose, R. and Bodenhausen, G. (2000) *J. Am. Chem. Soc.*, **122**, 1758–1761.

Clore, M.G., Szabo, A., Bax, A., Kay, L.E., Driscoll, P.C. and Gronenborn, A.M. (1990) *J. Am. Chem. Soc.*, **112**, 4989–4991.

Cornilescu, G., Marquardt, J.L., Ottiger, M. and Bax, A. (1998) *J. Am. Chem. Soc.*, **120**, 6836–6837.

Daragan, V.A. and Mayo, K.H. (1997) *Prog. Nucl. Magn. Reson. Spectrosc.*, **31**, 63–105.

Dayie, K.T. and Wagner, G. (1995) *J. Magn. Reson. Ser. B*, **109**, 105–108.

Deschamps, M. (2002) *J. Phys. Chem. A*, **106**, 2438–2445.

Deschamps, M. and Bodenhausen, G. (2001) *ChemPhysChem*, **8–9**, 539–543.

Felli, I.C., Richter, C., Griesinger, C. and Schwalbe, H. (1999) *J. Am. Chem. Soc.*, **121**, 1956–1957.

Frueh, D. (2002) *Prog. NMR Spectrosc.* **41**, 305–324.

Früh, D., Chiarparin, E., Pelupessy, P. and Bodenhausen, G. (2002) *J. Am. Chem. Soc.*, **124**, 4050–4057.

Früh, D., Tolman, J., Bodenhausen, G. and Zwahlen, C. (2001) *J. Am. Chem. Soc.*, **123**, 4810–4816.

Ghose, R. (2000) *Conc. Magn. Reson.*, **12**, 152–172.

Kloiber, K. and Konrat, R. (2000) *J. Biomol. NMR* **17**, 265–268.

Kloiber, K. and Konrat, R. (2000) *J. Biomol. NMR* **18**, 33–42.

Kroenke, C.D., Loria, J.P., Lee, L.K., Rance, M. and Palmer, A.G. (1998) *J. Am. Chem. Soc.*, **120**, 7905–7915.

Lipari, G. and Szabo, A. (1982) *J. Am. Chem. Soc.*, **104**, 4546–4558.

Loria, J.P., Rance, M. and Palmer, A.G. (1999) *J. Am. Chem. Soc.*, **121**, 2331–2332.

Meersmann, T. and Bodenhausen, G. (1995) *J. Magn. Reson.* **115**, 277–282.

Meiler, J., Prompers J.J., Peti, W., Griesinger, C. and Brüschweiler, R. (2001) *J. Am. Chem. Soc.*, **123**, 6098–6107.

Pang, Y. and Zuiderweg, E.R.P. (2000) *J. Am. Chem. Soc.*, **122**, 4841–4842.

Pang, Y., Wang, L., Pellechia, M., Kurochkin, A.V. and Zuiderweg, E.R.P. (1999) *J. Biomol. NMR* **14**, 297–306.

Pelupessy, P., Chiarparin, E., Ghose, R. and Bodenhausen, G. (1999) *J. Biomol. NMR*, **13**, 375–380.

Pelupessy, P., Chiarparin, E., Ghose, R. and Bodenhausen, G. (1999) *J. Biomol. NMR*, **14**, 277–280.

Peng, J.W. and Wagner, G. (1992) *J. Magn. Reson.*, **98**, 308–332.

Peti, W., Meiler, J., Brüschweiler, R. and Griesinger, C. (2002) *J. Am. Chem. Soc.*, **124**, 5822–5833.

Redfield, A.G. (1965) *Adv. Magn. Reson.*, **1**, 1–32.

Reif, B., Diener, A., Hennig, M., Maurer, M. and Griesinger, C. (2000) *J. Magn. Reson.*, **143**, 45–68.

Reif, B., Hennig, M. and Griesinger, C. (1997) *Science*, **276**, 1230–1233.

Skrynnikov, N.R., Konrat, R., Muhandiram, D.R. and Kay, L.E. (2000) *J. Am. Chem. Soc.*, **122**, 7059–7071.

Tessari, M. and Vuister, G. W. (2000) *J. Biomol. NMR*, **16**, 171–174.

Tjandra, N., Feller, S.E., Pastor, W.P. and Bax, A. (1995) *J. Am. Chem. Soc.*, **117**, 12562–12566.

Tjandra, N., Szabo, A. and Bax, A. (1996) *J. Am. Chem. Soc.*, **118**, 6986–6991.

Tolman, J. (2002) *J. Am. Chem. Soc.*, **124**, 12020–12030.

Tolman, J., Chiarparin, E. and Bodenhausen, G. (2000) *J. Am. Chem. Soc.*, **122**, 11523–11524.

Vijay-Kumar, S., Bugg, C.E. and Cook C.J.J. (1987) *J. Mol. Biol.*, **194**, 531–544.

Wokaun, A. and Ernst, R.R. (1978) *Mol. Phys.*, **18**, 317–341.

Yang, D. and Kay, L.E. (1998) *J. Am. Chem. Soc.*, **120**, 7905–7915.

Yang, D., Konrat, R. and Kay, L.E. (1997) *J. Am. Chem. Soc.*, **119**, 11938–11940.